Journal of Catalysis **202,** 229–244 (2001)
doi:10.1006/jcat.2001.3286, available online at http://www.idealibrary.com on IDEAL®

Lanthanum Chromite Based Catalysts for Oxidation of Methane Directly on SOFC Anodes

Joseph Sfeir,* Philippe A. Buffat,† Pedro Möckli,‡ Nicolas Xanthopoulos,§ Ruben Vasquez,* Hans Joerg Mathieu,§ Jan Van herle,* and K. Ravindranathan Thampi*,[1]

*Laboratory of Photonics and Interfaces, Department of Chemistry, †Interdepartmental Center of Electron Microscopy, Department of Material Science, ‡Laboratory of Ceramics, Department of Material Science, §Laboratory of Metallurgical Chemistry—Surface Analysis Group, Department of Material Science, Swiss Federal Institute of Technology (EPFL), CH-1015 Lausanne, Switzerland

Received November 27, 2000; accepted May 15, 2001; published online August 9, 2001

Catalytic properties of substituted lanthanum chromites were investigated for their use as anode materials for direct methane oxidation in solid oxide fuel cell (SOFC) anode materials. Different reaction mixtures were chosen to simulate the various SOFC operating conditions: partial oxidation, CO_2 reforming by recycling, and H_2O reforming. All experiments were performed in methane-rich atmospheres. Alkaline earth elements such as Ca, Sr, and Mg, and first series transition metals—Mn, Fe, Co, and Ni—were substituted into the $LaCrO_3$ lattice. Three different catalytic behaviors were observed depending on the substituents. The Ni-substituted powders showed the highest activity toward CH_4. Ni substitution showed also interesting H_2O and CO_2 reforming activities. For all catalysts, except in the case of Fe-substituted $LaCrO_3$, only a small amount of carbon was detected on the surface (1∼3 monolayers). Among the investigated *A*-site and *B*-site substitutents, Sr and Ni were found to be the most active and the most suitable substitutents for the $LaCrO_3$ SOFC anode purpose.

INTRODUCTION

Conventional solid oxide fuel cells (SOFC) are operated with pure hydrogen or fully or partially reformed natural gas. SOFC anodes are generally made of electrocatalytically active Ni–YSZ cermets. Pure methane feeding on this anode leads to the detachment of Ni particles from the YSZ support and their encapsulation by carbon. A temperature dependent steam-to-carbon ratio of 1.5∼1 is necessary to inhibit methane pyrolysis (1). From energetic, operational, and design considerations, SOFCs running on direct natural gas feed are more attractive systems. However, in this case, several parameters influence the anode performance and stability. The anodes should withstand reduction at P_{O_2} as low as 10^{-24} atm, be compatible with the YSZ electrolyte, possess acceptable conductivity and appropriate catalytic and electrocatalytic properties, and inhibit carbon deposition. There is growing evidence that materials with mixed electronic and ionic conductivity promote partial or even total oxidation of methane (2–6). Lanthanide perovskites of the first row transition metals have been investigated for catalytic combustion of gases, such as CO and CH_4. Of these oxides, $Ln MnO_3$, $Ln FeO_3$, $Ln CoO_3$, and $Ln NiO_3$ were found to exhibit interesting oxidative behavior under co-feed ($CH_4 + O_2$) reaction conditions, whereas $Ln CrO_3$ was least active (*Ln*: lanthanide) (5). However, of all these perovskites, $LaCrO_3$ was reported to be the most stable at 1000°C and very low oxygen partial pressures (≈10^{-21} atm), whereas $Ln MnO_3$, $Ln FeO_3$, $Ln CoO_3$, and $Ln NiO_3$ decomposed at a P_{O_2} of 10^{-15}, 10^{-17}, 10^{-7}, and 10^{-4} atm, respectively (7). The lanthanide part influences the catalytic activity less than the accompanying transition metal and the perovskite (ABO_3) stability reduces with decreasing size of the *A* cation, from La to Gd (2). One way to overcome this stability problem is to accommodate the active Mn, Fe, Co, and Ni species in a stable structure based on $LaCrO_3$. In this manner, a stable as well as catalytically active perovskite, with mixed conduction, could be produced.

In literature, $LaCrO_3$, $La_{0.8}Sr_{0.2}CrO_3$, and $LaCr_{0.8}Nb_{0.2}O_3$ were investigated as combustion catalysts in 2% CH_4 in air and were found to be the least active oxides among transition metal lanthanum perovskites (5, 6, 8–10). However, $La_{0.8}Sr_{0.2}CrO_3$ was found as the most active among $La_{0.8}Sr_{0.2}MO_3$ (M = Fe, Co, Mn, and Y) for the CO oxidation (2% CO in air) (5). The low activity for CH_4 oxidation was related to the poor ionic conductivity (5), low oxygen adsorption, and lattice oxygen nonavailability for the activation and oxidation of CH_4 (8, 11). Al_2O_3 and $MgAl_2O_4$ supported $LaCrO_3$ showed increased activity for CH_4 oxidation when compared to the unsupported $LaCrO_3$, in 1 : 4 : 95 $CH_4 : O_2 : N_2$ gas mixture (12). The increase in activity was explained by an increase of the dispersion state of the perovskite phase. Similarly, $LaCr_{1-x}Mg_xO_3$ ($x = 0 \sim 0.5$) were dispersed over MgO supports and high activities were observed in 1.5 : 18 : 80.5 $CH_4 : O_2$: He (13). The high dispersion of these catalysts (submicrometer powders of 15 ∼ 20 m^2/g surface area) as

[1] To whom correspondence should be addressed. E-mail: Ravindranathan.Thampi@epfl.ch. Fax: +41-21-6934111.

0021-9517/01 $35.00

well as the favorable adsorption energies for O_2 (between −168 and −188 kJ/mol) were thought to be relevant for the reaction. $LaCr_{1-x}Ni_xO_3$ catalysts were also investigated previously in 25 : 12.5 : 62.5 $CH_4 : O_2 : He$ (14). Again, oxygen adsorption and CH_4 activation were observed to affect the reaction. In general, the activity increased upon increased substitution of Ni as in the case of Mg. However, the supported perovskites ($LaCrO_3$ and $LaCr_{1-x}Mg_xO_3$) showed activities higher than the unsupported perovskites ($LaCrO_3$, $LaCr_{1-x}Mg_xO_3$, and $LaCr_{1-x}Ni_xO_3$). Baker *et al.* (15, 16) worked with *A*-site and *B*-site substituted $LaCrO_3$ ($La_{0.8}Ca_{0.2}CrO_3$ and $La_{0.8}Ca_{0.2}Cr_{0.9}(Co, Ni)_{0.1}O_3$) in 5 : 95 $CH_4 : He$ or 5 : 3 : 92 $CH_4 : H_2O : He$ mixtures. They found that these perovskites resisted much better to carbon deposition than a Ni–YSZ-cermet SOFC anode. Nevertheless, they observed carbon deposition at temperatures above 600°C, where methane cracking occurs. Water addition lowered the carbon formation. For the Co- and Ni-substituted $La_{0.8}Ca_{0.2}CrO_3$, they observed partial decomposition of the compounds. It is worth noting that all experiments on $LaCrO_3$-based perovskites reported in the literature used significantly diluted methane, whereas we worked under CH_4-rich conditions. Also, only Refs. (14–16) had the purpose of applying these materials as anodes for SOFCs.

Calcium-substituted lanthanum chromites were previously explored as alternative anodes to Ni–YSZ by the present authors (17). A small degradation was observed and was related to a progressive reduction of the electrode as well as a topotactic reaction between excess Ca or Sr with YSZ (17, 18). This reaction is however inhibited when low substitution levels are adopted (around 15% on the *A* site) (18). The lanthanum calcium and/or strontium chromite compounds were observed to inhibit coking, but their overall electrocatalytic activity was found to be low under pure methane feed (17). In this work, because of the stability of $LaCrO_3$ based materials, an attempt was made to increase their catalytic activity by substituting them with catalytically active Mn, Fe, Co, and Ni. Since we intend to use them for SOFC anode materials for direct methane feeding, different gas reaction mixtures were chosen to simulate the various SOFC operating conditions under catalytic conditions.

METHODS

Powder Preparation

Different lanthanum chromite powders were prepared through a modified citrate route (3), starting from nitrate precursors (Fluka, >99% purity except for $Cr(NO_3)_3 \cdot 9H_2O$ from Acros, 99%) and 1 M aqueous citric acid solution. Most of the water was removed by heating at 80–90°C in vaccum. The gels obtained were precalcined at 110°C for 20 h, then at 200°C for 2 h, and the resulting powders were crushed to size by dry ball-milling. A high-temperature calcination at 1100°C was then necessary to get pure perovskites, as confirmed by X-ray powder diffraction (17, 18). In order to tune the activity of the lanthanum chromite, different alkaline-earth and transition-metal substituents were considered: 15% for Ca and Sr (*A* site), and 10% for Mg, Mn, Fe, Co, and Ni (*B* site). Low substitution levels on the *A* site were used to prevent segregation of secondary phases (18). Ca and Sr also help to achieve good adhesion of chromites to the YSZ surface, which is necessary for the cell's mechanical stability and better current collection.

Surface area was measured using a BET Micrometrics Gemini 2375 apparatus (N_2 adsorption at 77 K). The particle size distribution was measured in a Horiba CAPA-700 analyzer.

Catalytic Tests

Fresh catalyst (0.2 to 0.5 g) was introduced in a quartz tube of 20 cm length (0.9 cm i.d.; 12 cm heated zone) and placed between two quartz wool plugs, as a 3-mm thick powder bed. A thermocouple protected in a quartz tube was placed in the catalyst bed and it served to monitor the powder temperature. The same catalyst was used for the whole series of gas compositions. All gas input and output lines of the reactor were heated to 150°C to prevent water condensation. This configuration is shown in Fig. 1. In order to assess the oxidation activities, different gas compositions were considered: a 5 : 1 $CH_4 : O_2$ mixture for the partial oxidation condition; a 5 : 1 : 0.6 $CH_4 : O_2 : CO_2$ mixture for CO_2 recycling-reforming behavior and 56 : y : x

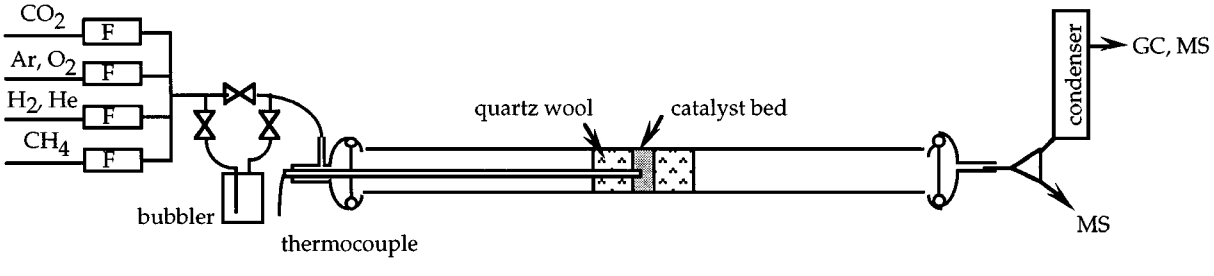

FIG. 1. Schematic view of the catalytic reactor. F represents the massflow controllers.

$CH_4 : Ar : H_2O$, $(x + y = 44)$, for steam reforming operation. CH_4, O_2, CO_2, Ar, and He feed rates were monitored by mass-flow controllers (Bronkhorst), whereas H_2O was saturated using a bubbler maintained at a controlled temperature. The gas flow rate was adjusted for an hourly space velocity of approximately 19000 h^{-1} (v/v). The system operated at atmospheric pressure and the inlet pressure was followed with a pressure gauge to monitor any flow blocking due to carbon build-up. Thiele modulus, gas film resistance calculations (19), as well as the experimentally observed gas mixture flow rates indicated no mass transfer limitations. Both the reaction products and the inlet gas mixtures were analyzed by gas chromatography (Carlo Erba MFC500 and Gowmac instruments) after water condensation. A Porapak Q column with He as carrier was used for Ar, CH_4, CO_2, and C_2 compound analysis, whereas a molecular sieve (5 Å) in Ar carrier was used for H_2, O_2, CH_4, and CO detection. Measurements were made at steady state conditions (approximately 1 h after temperature stabilization).

Temperature Programmed Oxidation and Reduction

At the end of each run, temperature programmed oxidation (TPO) in 20 ml/min He with 4 ml/min O_2 was undertaken in order to estimate the carbon deposition, after having cooled the reactor to room temperature in He (in typically 40 min time). An online quadrupole mass spectrometer (Residual Gas Analyser, Spectra, Leda Mass Vision, HF-100), which allowed a quantitative analysis of the outlet gas (CO, CO_2), was used for detection.

Temperature programmed reduction (TPR) of lanthanum chromite powders preoxidized at 900°C for 1 h was performed in 9% H_2 in Ar with a total flow rate of 55 ml/min. The water produced during this reaction was followed by the online mass spectrometer.

The heating rate for both TPO and TPR was set at 25°C/min.

XPS and TEM Analysis

Surface analysis was performed by X-ray photoelectron spectroscopy (XPS), in a Perkin–Elmer Phi 5500 and a Kratos Axis Ultra Instruments using Mg$K\alpha$ radiation in the first and Al$K\alpha$ in the second (except for the Mg-doped lanthanum chromite, where Al$K\alpha$ radiation was used). Samples were pressed on an indium sheet fixed on the sample holder. All spectra were analyzed and fitted using the instruments' softwares. Peak positions were corrected by shifting the $C1s$ peak to 285 eV. Labeling of the different Cr, La, and transition-metal elements was done by comparison with literature data. In the case of $La_{0.85}Ca_{0.15}Cr_{0.9}Ni_{0.1}O_3$, XPS analysis was performed before and after several Ar^+ sputtering steps, in order to estimate the surface enrichment of the powder.

TEM analysis was performed in a Philips EM430T instrument at 300 kV equipped with an EDS X-ray spectrometer. Carbon film on copper grids were impregnated by the powder dispersed in methanol.

RESULTS

Powder Characteristics and TPR

After ball-milling, lanthanum chromite powders showed a specific BET surface area between 1 and 3 m^2/g and a particle size distribution centered at 1 to 2.6 μm, as shown in Table 1.

Figure 2 shows TPR spectra for the different lanthanum chromite catalysts preoxidized at 900°C for 1 h. Two peaks were observed at 364–420 and 446–527°C depending on the substituent. The total amount of atomic O lost by reduction was calculated by integrating the water peaks measured by MS. The samples substituted with Ca and Sr were reduced by 0.08 and 0.06 O/ LC molecule, respectively. The calculated values correspond to $x/2$ $(x = 0.15)$, i.e., 0.075, and matches well with the experimental

TABLE 1

Summary of the Different Powders Characteristics as well as the Activation Energies E_a and Their Error Estimates in 5 : 1 $CH_4 : O_2$ and 56 : 41 : 3 $CH_4 : Ar : H_2O$ Gas Mixtures

Catalyst composition	Mass [g]	Surface area [m^2/g]	Particle size d_{50} [μm]	E_a 5 : 1 $CH_4 : O_2$ [kJ/mol]	E_a 3% H_2O [kJ/mol]
$La_{0.85}Ca_{0.15}CrO_3$	0.40	2.6	0.9	82 ± 4 (6)	173 ± 8 (4)
$La_{0.85}Ca_{0.15}Cr_{0.9}Mg_{0.1}O_3$	0.46	1.0	2.6	98 ± 7 (6)	192 ± 28 (5)
$La_{0.85}Ca_{0.15}Cr_{0.9}Ni_{0.1}O_3$	0.26	1.5	1.8	45 ± 1 (7)	127 ± 39 (4)
$La_{0.85}Sr_{0.15}CrO_3$	0.60	2.7	1.0	86 ± 40 (3)	182 ± 42 (4)
$La_{0.85}Sr_{0.15}Cr_{0.9}Mg_{0.1}O_3$	0.56	1.8	2.3	90 ± 5 (7)	164 ± 11 (5)
$LaCrO_3$	0.27	2.8	0.8	97 ± 5 (4)	272 ± 14 (3)
$LaCr_{0.9}Mg_{0.1}O_3$	0.21	3.0	1.3	116 ± 5 (4)	193 ± 9 (4)
$LaCr_{0.9}Mn_{0.1}O_3$	0.47	2.3	1.6	85 ± 5 (4)	116 ± 3 (3)
$LaCr_{0.9}Fe_{0.1}O_3$	0.49	2.0	1.1	98 ± 7 (4)	234 ± 26 (4)
$LaCr_{0.9}Co_{0.1}O_3$	0.31	1.4	2.1	121 ± 6 (6)	145 ± 15 (4)
$LaCr_{0.9}Ni_{0.1}O_3$	0.43	1.4	2.1	116 ± 1 (4)	43 ± 10 (4)

Note. The number of points used for the Arrhenius plots are given in parentheses.

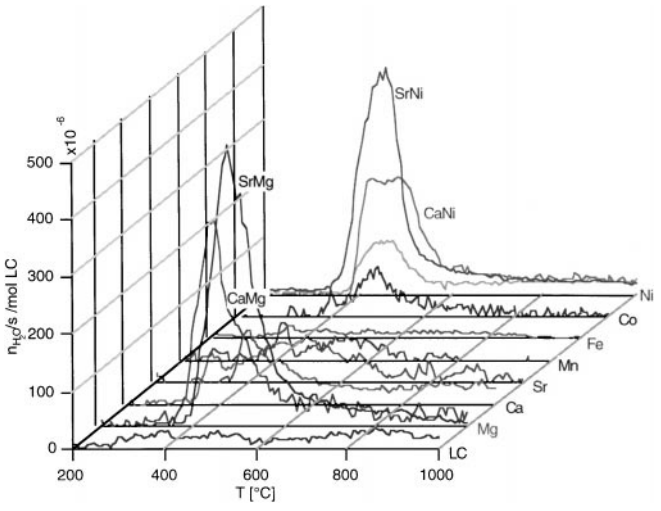

FIG. 2. Temperature programmed reduction in 9% H_2 in Ar with a total flow rate of 55 ml/min, and a heating rate of 25°C/min, of preoxidized lanthanum chromites.

results. The Mg, Mn, Fe, Co, and Ni substituted LCs were reduced to an equivalent of 0.09, 0.026, 0.025, 0.031, and 0.064 O/LC molecule compared to a calculated value of 0.05 ($x/2$, $x = 0.1$) if the dopant is divalent. LC gave an amount of 0.02 O/molecule of LC. Estimated values of the nonstoichiometry (δ), based on reference (20) thermogravimetric measurements, obtained by subtracting the measured δ of the $La_{0.7}Ca_{0.3}Cr_{0.9}M_{0.1}O_3$ (M = transition elements) powders from the base material $La_{0.7}Ca_{0.3}CrO_3$, amount to 0.02, 0.06, 0.04, 0.03, 0.07, and 0.07 for the Mg, Ca, Mn, Fe, Co, and Ni substitution, respectively. These values are higher, for the transition metals, than in our measurements. Overall, our results indicate that Fe and Mn ($\delta = 0.025$ and 0.026) are in the trivalent state while Co ($\delta = 0.031$) has mixed valencies (III and II), whereas Ni is in the divalent state. A double substitution of the A and B sites gives rise to a higher degree of reduction: 0.09 for Ca–Ni, 0.14 for Sr–Ni, 0.124 for Ca–Mg, and 0.155 for Sr–Mg substitution, respectively, compared with the expected nominal value of 0.125. This indicates that the transition metal substituted LCs do not decompose and that in the special case of $LaCr_{0.9}Ni_{0.1}O_3$ and $La_{0.85}Ca_{0.15}Cr_{0.9}Ni_{0.1}O_3$, Ni^{II} does not undergo a further reduction. Moreover, part of the water produced by TPR should be attributed to adsorbed hydroxyl groups and surface oxgen (3). The low temperature shoulder corresponds to absorbed or adsorbed surface oxygen, whereas the high temperature shoulder is assigned to lattice oxygen (3). Generally, the two former adsorbed species desorb more easily from Ca than from Sr and transition-metal substituted LCs. For the transition elements the reduction starts at almost the same temperature. Lattice oxygen seems to be more stabilized by Sr > Ca > Mg. For the transition elements, lattice oxygen is more easily removed and follows the order Mn > Ni > Co.

Effect of O_2

Figure 3a shows the steady state curves obtained by reacting 5:1 $CH_4:O_2$ gas mixture on various catalysts. The reactions start in the range between 300° and 600°C, depending on the nature of the substituent in $LaCrO_3$ (LC). In this low temperature part of the curves, O_2 is entirely consumed by CH_4 to form CO_2 and H_2O (low CO and H_2 selectivities), thus showing total oxidation (reaction [1]). The CH_4 conversion reaches here a maximum of 10%, O_2 being the limiting factor in the

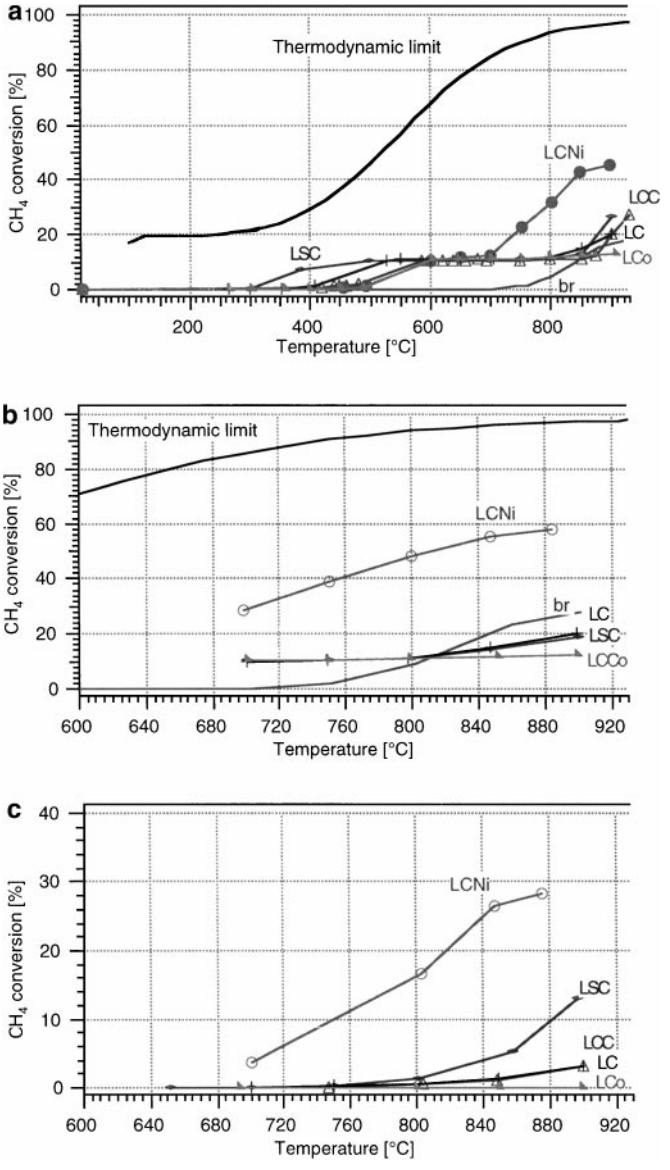

FIG. 3. Percent CH_4 conversion with temperature for the following gas mixtures: (a) 5:1 $CH_4:O_2$; (b) 5:1:0.6 $CH_4:O_2:CO_2$; and (c) 56:41:3 $CH_4:Ar:H_2O$. (br) represents the blank reactor and the solid line corresponds to the theoretical methane conversion taking carbon deposition into account.

reactions

$$CH_4 + 2O_2 = CO_2 + 2H_2O \quad [1]$$

$$CH_4 + \tfrac{1}{2}O_2 = CO + 2H_2. \quad [2]$$

It is only above 700°C that an observable net partial oxidation occurs (reaction [2]). Tests carried out in the blank reactor, under the different gas mixtures, showed no reaction occurring in the gas phase below 700°C, while at higher temperatures, the gases reacted to produce CO_2, CO, and H_2O; CO is also formed by water gas shift reaction

$$CO_2 + H_2 = CO + H_2O \quad [3]$$

with methane conversion reaching 15%, at 900°C, for the blanck reactor. On these curves, the thermodynamic limits are also shown. The gas phase thermodynamic equilibrium calculations were made using 13 different reactions taking into account H_2, CO, and CH_4 conversion, the methane–H_2O and CO_2 reforming reactions, the shift reaction, the dissociation reactions of CO, CO_2, and CH_4 to C as well as the Boudouard reaction. In these calculations, graphite was considered as the most stable carbon species. The high level of methane conversion observed in these calculations is due to carbon deposition under low oxidizing conditions. It is clearly seen that the calculated conversion in the 5:1 $CH_4:O_2$ gas mixture differs much from the experimental results, indicating low coking levels on the lanthanum chromites oxides.

All catalysts had their temperatures cycled from room temperature to 900°C and then back to ambient in order to verify the reproducibility of steady state values. In some cases, a hysteresis in % CH_4 conversion occurred, whereby a higher conversion was noticed during cooling at a given temperature when compared to the heating cycle.

In order to compare the activity of various catalysts, the oxidation behavior of lanthanum chromites was evaluated at the temperature at which 50% O_2 conversion occurs. It is observed that among the alkaline earth elements, Sr ($T \approx 390$°C) is best for promoting oxidation, whereas Mg impedes it (550°C), with Ca at an intermediate level ($T \approx 500$°C), when compared to pure LC ($T \approx 450$°C). The same trend is reported in the literature (6) for Ca or Sr substituted $LaMO_3$ (M = Mn, Fe, Co) combustion catalysts. Since $La_{0.85}Ca_{0.15}CrO_3$ and $La_{0.85}Sr_{0.15}CrO_3$ have the same surface areas and particle size distributions (Table 1), this behavior seems to be independent of such parameters. A double substitution Ca and Mg or Sr and Mg shifted the temperature to higher values, compared to Mg substitution alone ($T \approx 570$°C for $La_{0.85}Ca_{0.15}Cr_{0.9}Mg_{0.1}O_3$; $T \approx 620$°C for $La_{0.85}Sr_{0.15}Cr_{0.9}Mg_{0.1}O_3$). For the various transition-metal elements, the observed trend was as follows: Fe (475°C) < Mn (500°C) < Co ≈ Ni (540°C). This trend is also qualitatively followed when the activity is evaluated on the basis of methane conversion and product selectivities, where three different patterns are distinctly noticed with our catalysts:

1. Case A. $La_{0.85}Sr_{0.15}Cr_{0.9}Mg_{0.1}O_3$ (LSrCMg) $La_{0.85}Ca_{0.15}Cr_{0.9}Mg_{0.1}O_3$ (LCaCMg), $La_{0.85}Cr_{0.9}Mg_{0.1}O_3$ (LCMg), and $LaCr_{0.9}Co_{0.1}O_3$ (LCCo), showed complete oxidation (reaction [1]) at high temperatures, exhibiting a negative catalytic effect when compared to the blank reactor (br) alone or the base material $LaCrO_3$ (LC), possibly by inhibiting the radical reactions in the gas phase;

2. Case B. $La_{0.85}Ca_{0.15}CrO_3$ (LCaC), $LaCr_{0.9}Mn_{0.1}O_3$ (LCMn), $LaCr_{0.9}Fe_{0.1}O_3$ (LCFe), and $LaCrO_3$ (LC) catalysts showed activities similar to that of the blank reactor and indicated a preference for water–gas shift (reaction [3]) at high temperatures;

3. Case C. $La_{0.85}Sr_{0.15}CrO_3$ (LSrC), $LaCr_{0.9}Ni_{0.1}O_3$ (LCNi), and $La_{0.85}Ca_{0.15}Cr_{0.9}Ni_{0.1}O_3$ (LCaCNi) significantly favored the reforming reaction at high temperatures with an increase in the methane conversion and CO and H_2 selectivities, the reforming being almost complete according to reaction [2] for the Ni containing compounds above 800°C.

In terms of turn-over frequency (TOF), calculated as the number of moles of CH_4 reacted per second per unit surface area of the catalyst, regardless of product selectivity, the classification at 850°C follows the order of substitution Ca < Sr < Mg < Mn < LC < Fe < Co < CaMg < SrMg < Ni < CaNi. Table 2 summarizes the activity of the

TABLE 2

Summary of CH_4 Conversion in Percent for the 5:1 $CH_4:O_2$, 5:1:0.6 $CH_4:O_2:CO_2$, and 56:20:24 $CH_4:Ar:H_2O$ Gas Mixtures

Catalyst composition	% methane conversion (in parentheses: number of carbon monolayers)		
	5:1 $CH_4:O_2$	$CH_4:O_2:CO_2$	$CH_4:H_2O$
Maximum conversion possible	40[a]	52[b]	24[c]
$La_{0.85}Ca_{0.15}CrO_3$	10.7 (0.6)	−(0.0)	0.39 (2.2)
$La_{0.85}Ca_{0.15}Cr_{0.9}Mg_{0.1}O_3$	11.2 (—)	10.2 (—)	0.04 (—)
$La_{0.85}Ca_{0.15}Cr_{0.9}Ni_{0.1}O_3$	36.7 (0.7)	37.8 (0.8)	18.70 (3.3)
$La_{0.85}Sr_{0.15}CrO_3$	11.3 (0.0)	10.9 (0.0)	1.22 (0.4)
$La_{0.85}Sr_{0.15}Cr_{0.9}Mg_{0.1}O_3$	10.9 (0.0)	10.8 (0.0)	0.22 (0.0)
$LaCrO_3$	11.8 (0.3)	11.1 (0.5)	0.50 (1.7)
$LaCr_{0.9}Mg_{0.1}O_3$	13.1 (1.7)	12.4 (1.5)	0.05 (1.1)
$LaCr_{0.9}Mn_{0.1}O_3$	11.2 (0.0)	11.0 (0.0)	0.79 (1.1)
$LaCr_{0.9}Fe_{0.1}O_3$	13.1 (2.6)	12.0 (0.5)	0.62 (69.4)
$LaCr_{0.9}Co_{0.1}O_3$	11.5 (0.0)	11.1 (0.0)	0.21 (0.0)
$LaCr_{0.9}Ni_{0.1}O_3$[d]	32.1 (0.4)	48.2 (—)	16.6 (1.9)

Note. Summary of the TPO analysis after the different runs is given in parentheses; Units of the TPO are given in monolayers of carbon reported to the powder surface area; (—) not measured.

[a] $CH_4 + 0.5O_2 = CO + 2H_2$.

[b] $CH_4 + 0.5O_2 = CO + 2H_2$ and $CH_4 + CO_2 = 2CO + 2H_2$.

[c] $CH_4 + H_2O = CO + 3H_2$.

[d] Activity after 20 h run.

different catalysts at 800°C. Activities of all catalysts were stable over one day or more, except for Ni-containing LC (case C). In the latter, the initial conversion was low and comparable to that of LCCo (10% CH_4 conversion). The activity increased over a period of 20 h and reached full reforming level of about 40% CH_4 conversion (5 : 1 $CH_4 : O_2$ initial mixture), at 900°C. This activity is sustained for more than 360 h at 800°C.

Apparent activation energies for the oxidation reactions were determined at conversions below 10%. Error limits were calculated from the error of the slope of the Arrhenius plot. They vary between 82 and 121 kJ/mol (Table 1). They are in general agreement with data published for different gas compositions: 101 (2 : 1 : 5 $CH_4 : O_2$: He) to 120.4 kJ/mol (2 vol% CH_4 in air) for $LaCrO_3$ (6, 14), 120 to 147 kJ/mol for $La_{0.8}Ca_{0.2}CrO_3$ (5% CH_4 in He) (15), 90 to 100 kJ/mol for $LaCr_{0.75}Ni_{0.25}O_3$ (2 : 1 : 5 $CH_4 : O_2$: He) (14), and 91.1, 92.4, and 76.1 kJ/mol for $LaMnO_3$, $LaCoO_3$, and $LaFeO_3$ (2 vol% CH_4 in air) (6), compared to 115.4 kJ/mol for Pt (1 wt%) Al_2O_3 and 257.1 kJ/mol for the noncatalytic thermal reaction (6).

Effect of CO_2

Figure 3b shows the influence of CO_2 on the oxidation reaction of methane (5 : 1 : 0.6 $CH_4 : O_2 : CO_2$ gas mixture). Table 2 summarizes the activity of the different catalysts at 800°C. It is observed that in all catalysts, except the Ni-containing compounds, CO_2 reforming is small at high temperature. The curves follow the same steady-state trend as with the 5 : 1 $CH_4 : O_2$ runs, and at $T \geq 750$°C the gas-shift reaction (reaction [3]) takes place over some catalysts by a concomitant increase in CO and decrease in H_2 selectivity. Separate experiments in 5 : 1 : 0.6 $CH_4 : Ar : CO_2$ (without O_2) confirmed the low CO_2 reforming ability of these materials. On the other hand, almost full CO_2-reforming,

$$CH_4 + CO_2 = 2CO + 2H_2, \qquad [4]$$

took place on LCNi, LCaCNi, and to some extent on LSrC (all materials of case C mentioned above). CO_2 reforming is relevant for SOFC operations, where a fraction of the product CO_2 could be recycled along with the natural gas feed.

Effect of H_2O

Figure 3c displays the steam reforming reaction in a 56 : 20 : 24 $CH_4 : Ar : H_2O$ mixture and Table 2 summarizes the activity of the different catalysts at 800°C in a 56 : 41 : 3 $CH_4 : Ar : H_2O$ gas mixture. Here again, we observe three different behaviors depending on the catalyst composition as recorded for the oxidation of methane. In most cases, CH_4 conversion is very low ($\leq$1%, see Table 2) and quite independent of the water content. The reaction order with respect to P_{H_2O} varied with temperature, changing from a positive order at high temperatures to a negative order at low temperatures. It was near zero for the cases where steam had little effect on the reaction (case A materials). LC, LSrC, and LCMn are slightly affected by water (case B materials), whereas the Ni-containing powders show high conversion of water at $T \geq 800$°C (case C) following the overall reaction

$$CH_4 + H_2O = CO + 3H_2. \qquad [5]$$

The CO selectivity diminishes in all cases when the water content is increased from 3 to 23%, indicating that the reverse water–gas shift reaction [3] is fast. Table 3 summarizes the CO selectivities at 900°C in 56 : 20 : 24 and 56 : 41 : 3 $CH_4 : Ar : H_2O$.

TABLE 3

CO Selectivity as a Function of the Steam Content in the 56 : x : y ($x + y = 44$) $CH_4 : Ar : H_2O$ Gas Mixture at 900°C

	CO selectivity	
Powder versus CO selectivity	24% H_2O	3% H_2O
$La_{0.85}Ca_{0.15}CrO_3$	0	99
$La_{0.85}Ca_{0.15}Cr_{0.9}Mg_{0.1}O_3$	0	33
$La_{0.85}Ca_{0.15}Cr_{0.9}Ni_{0.1}O_3$	81	100
$La_{0.85}Sr_{0.15}CrO_3$	65	100
$La_{0.85}Sr_{0.15}Cr_{0.9}Mg_{0.1}O_3$	0	42
$LaCrO_3$	10	96
$LaCr_{0.9}Mg_{0.1}O_3$	0	0
$LaCr_{0.9}Mn_{0.1}O_3$	36	80
$LaCr_{0.9}Fe_{0.1}O_3$	36	91
$LaCr_{0.9}Co_{0.1}O_3$	0	0
$LaCr_{0.9}Ni_{0.1}O_3$	88	100

Apparent activation energies in 56 : 41 : 3 $CH_4 : Ar : H_2O$ were calculated at conversions below 10% (see Table 1). They vary between 43 and 272 kJ/mol and depend on the fraction of water vapor, where the values tend to be higher with increasing steam content. Steam reforming on Ni-based catalysts is reported to have an activation energy between 20 and 160 kJ/mol (21), the latter representing the activation energy in the absence of diffusion limitations (22).

Methane Coupling

Only small amounts ($\leq$1%) of C_2 compounds (C_2H_2, C_2H_4, and C_2H_6) were observed in almost all cases for the oxidative coupling environment of 5 : 1 $CH_4 : O_2$ with the exception of Mg-substituted LC (16 to 24% at 900°C), the blank reactor (22% at 900°C, 56% at 700°C), LCCo (7% at 900°C), and LCaC (5% at 900°C). CO_2 increases slightly the coupling reaction, while in the blank reactor it rises to 82% at 900°C. H_2O addition suppresses C_2 compound formation totally except for the case of Mg-substituted LCs, where it only decreases (from 73 to 45% for LCaCMg, 33

to 19% for LSrCMg, and 23 to 19% for LCMg when passing from 56 : 20 : 23 to 56 : 41 : 3 $CH_4 : Ar : H_2O$). This illustrates the low methane oxidative coupling activity of these catalysts.

TPO

Temperature programmed oxidation (TPO) experiments were started from room temperature to 1000°C after running the catalytic reactions for about one day or more. They show that in all cases, except for LCFe, the amount of carbon estimated was less than $2 \sim 3$ monolayers (results are summarized in Table 2), normalized to the total surface of the catalysts. In the case of LCaCNi a total of 2 monolayers was estimated by integrating the CO_2 peaks signal after the run in 5 : 1 $CH_4 : O_2$ (360 h). In 56 : 41 : 3 $CH_4 : Ar : H_2O$, 3.3 and 3.5 monolayers were deposited on the same catalyst after 30 and 160 h, respectively, indicating that the total amount of carbon deposited did not change much. Similarly, measurements done on LCaC with dry and wet methane, showed that the total amount of carbon deposited with time tended to level off to a monolayer indicating that, at that point, the rate of coking might be equal to that of gasification of carbon or that all the catalytically active sites for coking are blocked by the deposited carbon. Thus, apart from the Fe-substituted LC, the other catalysts do not seem to build up carbon.

From these TPO experiments, different peaks of CO_2 have been observed at around 300, 400, 500–600, 700–800, and 900°C, corresponding to different types of carbon deposits, some being more stable than others. They may be related to the different carbon species reported by Rostrup-Nielsen (21) and Bartholomew (23) for Ni: adsorbed atomic (dispersed, surface carbide), bulk carbide, polymeric amorphous filaments or films, vermicular and graphitic (crystalline, films) carbon which react with H_2 in temperature programmed reaction hydrogenation (TPRH) at 200, 400, 400–600, and 550–850°C.

XPS Analysis

XPS analysis was conducted on freshly prepared powders as well as on used catalyst samples. The measurements were done on an area of approximately 100 μm^2. The XPS peak positions for the different elements were adjusted by shifting the carbon 1s peak to 285 eV. After deconvolution, average peak positions are: $3d_{5/2}$ La_I, 834.5 eV and La_{II} 838.5 eV; $2p_{3/2}$ Cr_I 576 eV and Cr_{II} 579 eV; $2p_{3/2}$ Ca 346.4 eV; $3d_{5/2}$ Sr 133.8 eV; $2p_{3/2}$ Mn 642.2 eV; $2p_{3/2}$ Fe 711 eV; $2p_{3/2}$ Co 780.5 eV; O_I 529.1 eV and O_{II} 531 eV. $2p_{3/2}$ Ni peak could not be resolved because it overlapped with La 3*d* peaks. As no Ni satellite peak existed around 870 eV we concluded that the surface concentration on the Ni-substituted LCs was below the detection limit (≈1%). La and Cr peaks remain at the same position independently of the substitution. The O 1*s* peaks, O_I and O_{II}, fluctuate slightly with the substitution. The binding energy of O_I decreases from Mn to Ni and from Mn to Ca while for O_{II} it increases from Mn to Ni, whereas it is almost unchanged for Ca and Sr (illustrated in Fig. 4).

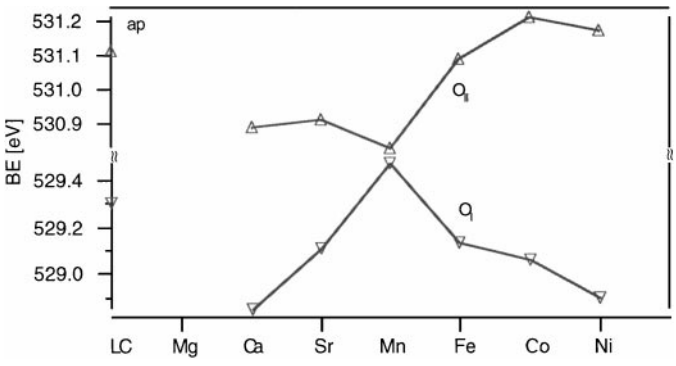

FIG. 4. The evolution of the O1*s*, O_I and O_{II} binding energies as a function of the substituent, for unreacted powders; (ap) as prepared.

The concentration of the different species are summarized in Table 4. It is seen that in all cases but the LC, LCC, LCCNi, and LSC powders, La is present in excess. This could stem from the preparation procedure. Next, Ca and Sr are seen to segregate strongly on the surface. This segregation is enhanced after the catalytic runs (from 10 to 22% for Ca and 10 to 14% for Sr). Ca seems to segregate more easily than Sr. In the case of a fresh $La_{0.85}Ca_{0.15}Cr_{0.9}Ni_{0.1}O_3$ powder, the La, Cr, and Ca peaks vary with time after sputtering with Ar^+; after 2 min sputtering time, the La, Cr, and Ca concentrations pass successively from 39 to 49%, 49 to 42%, and 12 to 9%, respectively. The gas atmosphere is observed to have an effect on the surface segregation of Ca as observed on LCaCNi samples exposed at 800°C to air, CO_2, or $H_2 + 3\% H_2O$ atmospheres for more than 100 h (bottom of Table 4). Wet hydrogen increases the segregation of Ca.

TEM Analysis

TEM analyses were performed on the LCNi, LCaCNi, and LCFe powders before and after catalysis. It was observed that in the case of LCaCNi, carbon formation was limited to some LCaCNi grains with small islets of Ni attached to them, as illustrated in Fig. 5a. These Ni islets have a mean particle size of 20 to 50 nm. The carbon is deposited around the Ni islets on the LCaCNi surface and forms well defined graphitic films, shown in Fig. 5b. These have a thickness of around 5 nm and seem to grow parallel to the surface of LaCaCNi particles. Some of the films were observed to be amorphous in electron diffraction mode. The particles free of Ni islets do not grow any carbon films. The composition of LCaCNi, measured on a large number of grains, does not change for particles with or without the Ni islets within accuracy of EDS microanalysis (50 s acquisition time). Ni islets are found on the free surface of LCaCNi and in some cases in the bottle neck between two grains. The origin of

TABLE 4

Summary of the XPS Surface Analysis Given in Percent of the Sum of the Total Metal Elements. ap: as Prepared; ac: after Catalysis

XPS analysis [%] Catalyst composition	La/Cr	Mg	Ca	Sr	Mn	Fe	Co	Ni *	Ca, Sr nominal	Mg, Mn, Fe, Co, Ni nominal
$LaCrO_3$, ap	0.9									
$LaCr_{0.9}Mg_{0.1}O_3$, ap	2.9	5.3								5
$LaCr_{0.9}Mg_{0.1}O_3$, ac	2.8	4.9								5
$La_{0.85}Ca_{0.15}CrO_3$, ap	1.0		10						7.5	
$La_{0.85}Ca_{0.15}CrO_3$, ac	1.0		22						7.5	
$La_{0.7}Ca_{0.32}CrO_3$, ap	1.0		39						16	
$La_{0.85}Sr_{0.15}CrO_3$, ap	0.9			10					7.5	
$La_{0.85}Sr_{0.15}CrO_3$, ac	0.8			14					7.5	
$LaCr_{0.9}Mn_{0.1}O_3$, ap	1.2				5					5
$LaCr_{0.9}Mn_{0.1}O_3$, ac	1.3				5.7					5
$LaCr_{0.9}Fe_{0.1}O_3$, ap	1.1					7.3				5
$LaCr_{0.9}Fe_{0.1}O_3$, ac	1.2					8.7				5
$LaCr_{0.9}Co_{0.1}O_3$, ap	1.2						1.9			5
$LaCr_{0.9}Co_{0.1}O_3$, ac	1.3						2.8			5
$LaCr_{0.9}Ni_{0.1}O_3$, ap	1.6							?		5
$LaCr_{0.9}Ni_{0.1}O_3$, ac	1.9							?		5
$La_{0.85}Ca_{0.15}Cr_{0.9}Ni_{0.1}O_3$, ap	1.0		10					?	7.5	5
$La_{0.85}Ca_{0.15}Cr_{0.9}Ni_{0.1}O_3$, ac	0.8		21					?	7.5	5
$La_{0.85}Ca_{0.15}Cr_{0.9}Ni_{0.1}O_3$, H_2	1.2		15					?	7.5	5
$La_{0.85}Ca_{0.15}Cr_{0.9}Ni_{0.1}O_3$, CO_2	1.0		9					?	7.5	5
$La_{0.85}Ca_{0.15}Cr_{0.9}Ni_{0.1}O_3$, air	1.2		6					?	7.5	5

Note. ap, as prepared; ac, after catalysis; *, Ni peak could not be resolved because of overlapping with La 3*d* peaks.

free Ni is not very clear, but it was possible to observe it on top of what seems to be a $CaCr_2O_4$ phase. This is shown in Figs. 6a and 6b. This phase is known to be one of the impurity phases that forms during the fabrication of Ca substituted LCs (18). Another impurity is the $CaCrO_4$ phase shown in Figs. 7a and 7b. On the LCNi powders, no Ni islets were observed.

LCFe did not show any Fe segregation of any kind. Chemical analysis measurements done on a large number of grains showed very similar compositions. The carbon deposition and its structure depends on the temperature of the reaction. Figures 8a and 8b show two different carbons after the run in 56 : 41 : 3 CH_4 : Ar : H_2O at 850°C. A major component is the soot-like carbon which is deposited in many cases on kinks. The other carbon represent amorphous films which have thicknesses of about 30 nm. However, the carbon coverage is low at 850°C. Running the catalyst at 900°C leads to structured graphitic films (see Fig. 8c) along with graphitic filaments (see Fig. 8d) running from the surface of the grains. From the TEM micrograph these filaments may build up epitaxially to the surface of the LCFe powder.

DISCUSSION

In XPS spectra, the $2p_{3/2}$ Mn peak is located at 642.2 eV, which is close to that of Mn^{III} (641.9 eV) (24). Fe seems to be in the trivalent state as its binding energy (BE) is in the range 710.5 to 711.7 eV (711.3 eV for Fe_2O_3, (25)). The BE of Co corresponds to both Co^{II} and Co^{III} (26). With Ni, however, no peak was observed. Overall, these results corroborate well with measured TPR spectra where mixed valencies were observed for Co ($\delta = 0.031$) and a valency of III for Mn and Fe as δ is close to that of LC. From TPR, Ni is thought to be in the divalent state.

The two observed Cr peaks can be assigned to Cr^{III} (576.1 eV, (25)) and Cr of a higher valency (579 eV). The high valency Cr can be either Cr^{IV} or surface Cr where its coordination sphere is not complete (3).

The two peaks of oxygen can be attributed to lattice oxygen O_I (529 eV) and to adsorbed oxygen and hydroxyl O_{II} (531 eV) (3)—it was not deconvolved into two further peaks because of overlapping. This agrees well with the TPR results where two peaks were observed, one for the surface adsorbed oxygen species and another for the lattice oxygen. The lattice oxygen O_I binding energy seems to decrease from Mn to Ni (see Fig. 4) as expected from the stability of the $LaMO_3$ oxides (7), indicating that oxygen vacancies are easily formed on Ni-substituted LCs compared to other substitutions. Also, O_I BE increases from Ca to Sr. From thermodynamic calculations based on values in the literature (27, 28), Sr-substituted LC reduces however more readily than Ca with a difference of ≈11 kJ/mol (for $x = 0.15$) (29). The O_{II} peak increases from Mn to Ni, with Mn having the lowest BE. This corroborates well with TPR measurements and indicates that oxygen adsorbs strongly on the Ni ≈ Co > Fe > Mn-substituted LCs. However, the

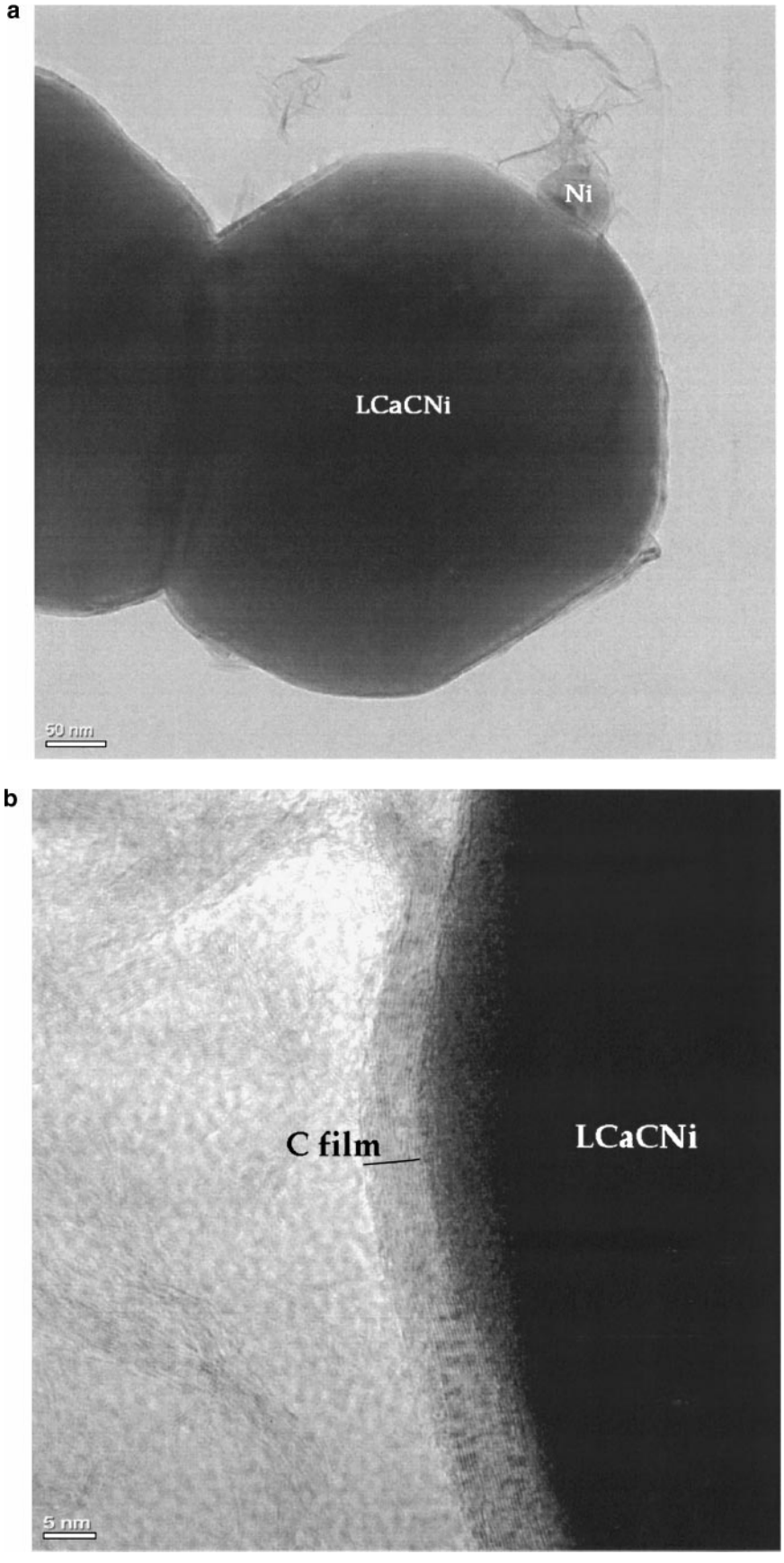

FIG. 5. TEM micrographs showing: (a) a Ni islet on top of a LCaCNi grain; (b) the carbon film around the grain.

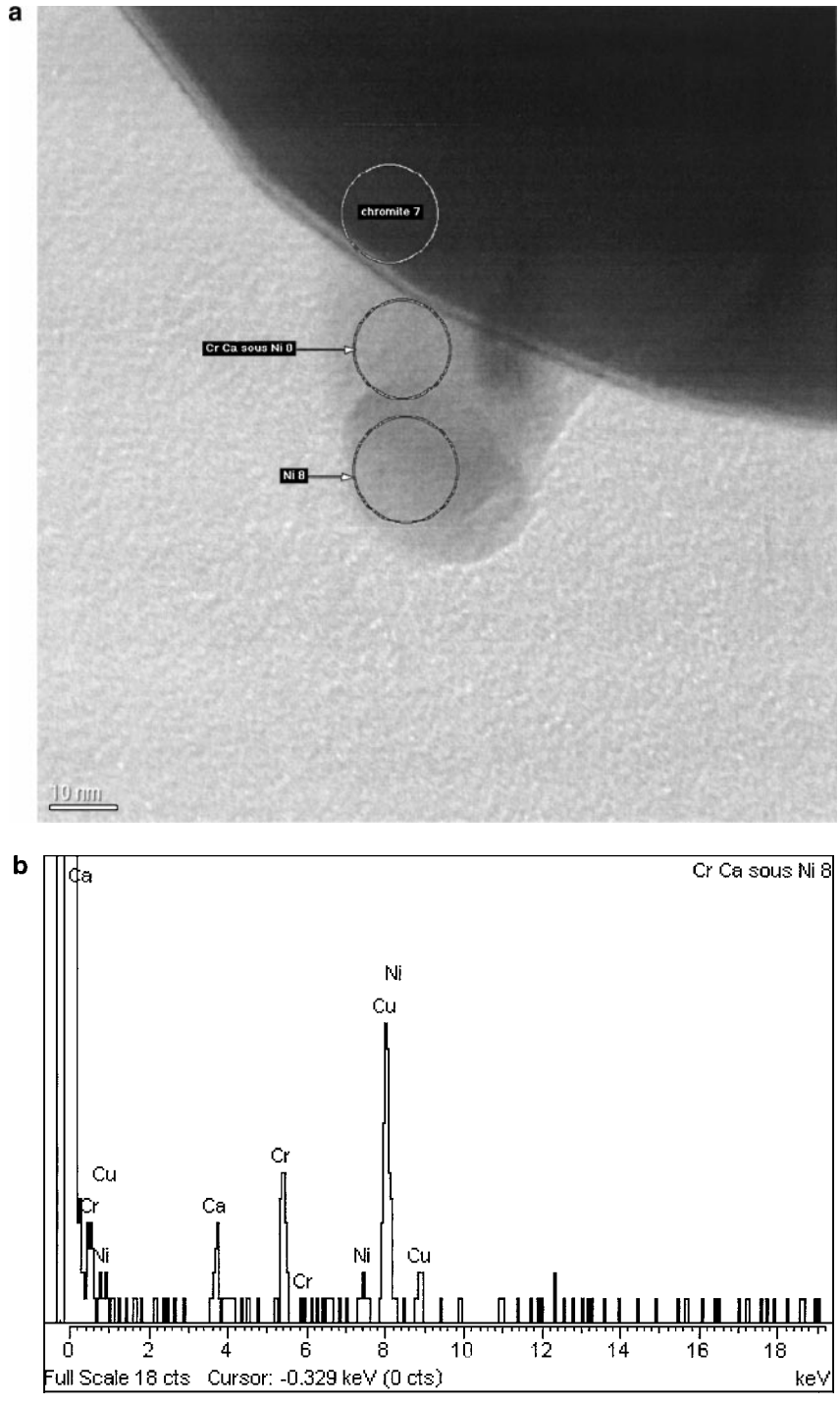

FIG. 6. LCaCNi powder after catalytic runs in 56 : 41 : 3 CH_4 : Ar : H_2O: (a) TEM micrograph of a Ni islet on top of a calcium chromate secondary phase; (b) EDS analysis of the same calcium chromate phase showing a concentration of 68% of Cr and 32% of Ca corresponding most probably to $CaCr_2O_4$ (copper is a signal from the bulky bars of the Cu grid).

total amount of O1*s* does not change for the different substituents. From TPR, the Sr substitution causes more oxygen to desorb than does Ca substitution. This difference in desorption could explain the higher activity of LSrC when compared to LCaC (50% O_2 conversion at 390°C for Sr- versus 500°C for Ca-substituted LC, and TOF of 3.9×10^{-9} for Sr versus 3.5×10^{-9} for Ca at 850°C in 5 : 1 $CH_4 : O_2$) as more oxygen from the lattice is available for the reaction. This effect is also observed on the doubly substituted LC (Sr or Ca/Mg and Sr or Ca/Ni). For the transition

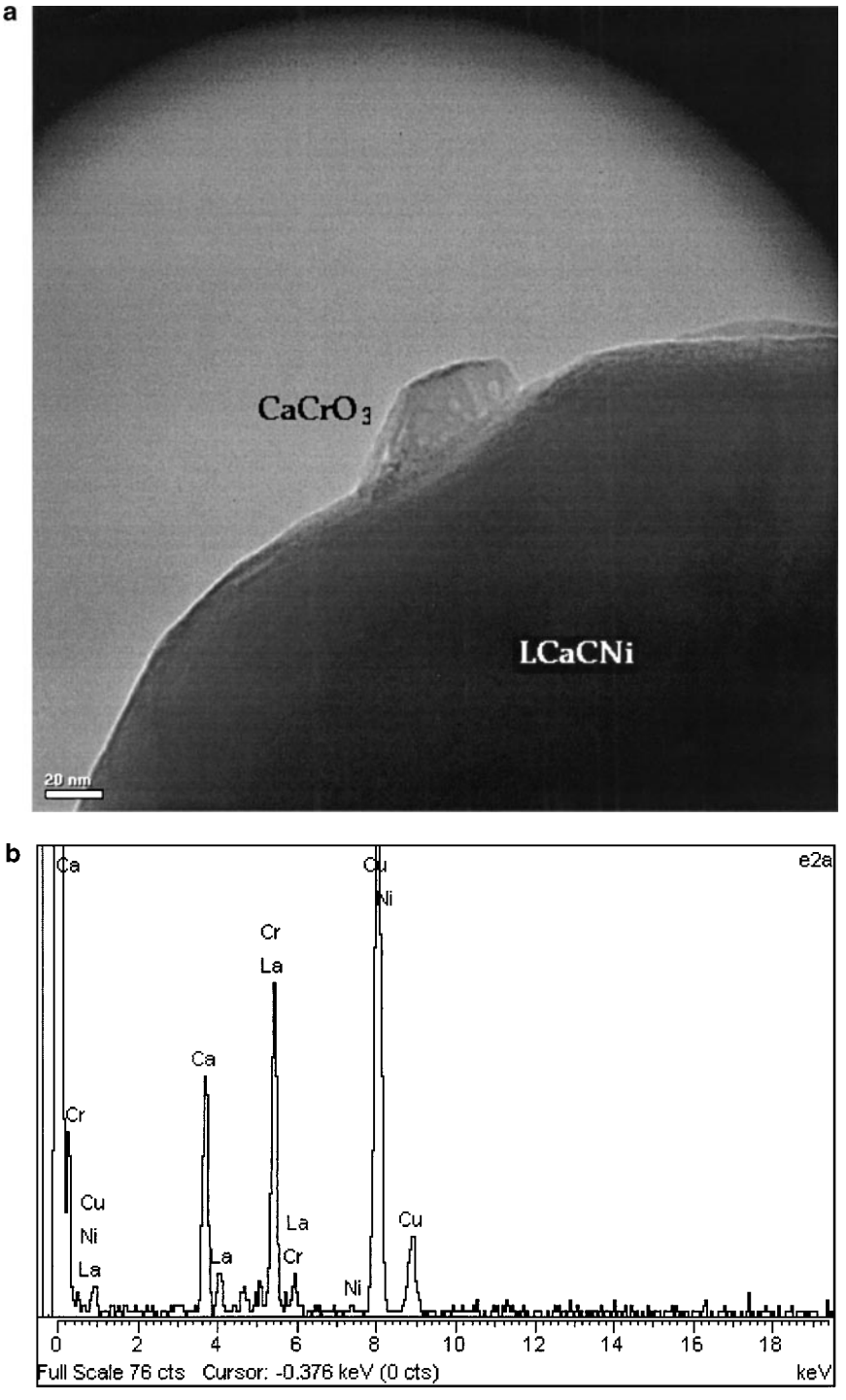

FIG. 7. LCaCNi powder: (a) TEM micrograph of a secondary phase corresponding to (b) $CaCrO_3$ as shown by EDS (50% Ca, 50% Cr). Copper is a signal from the bulky bars of the Cu grid.

elements, the TOF for Mn, Fe, Co, and Ni are 3.1, 5.6, 8.0, and 19.5×10^{-9}. This agrees well with the total amount of oxygen species desorbed by TPR (Mn 0.026 $\approx$ Fe 0.025 $<$ Co 0.031 $<$ Ni 0.064) and the O_I BE trend. This suggests that a relation exists between the reducibility and the catalytic activity on these oxides.

Surface concentration of the different elements show that surface segregation is important for Ca and Sr substitution. The Ni islets, observed on the LCaCNi powders, are most probably related to the liquid phases (calcium chromates) produced during sintering as the LCNi powder did not present any free Ni. Two secondary phases, $CaCrO_3$

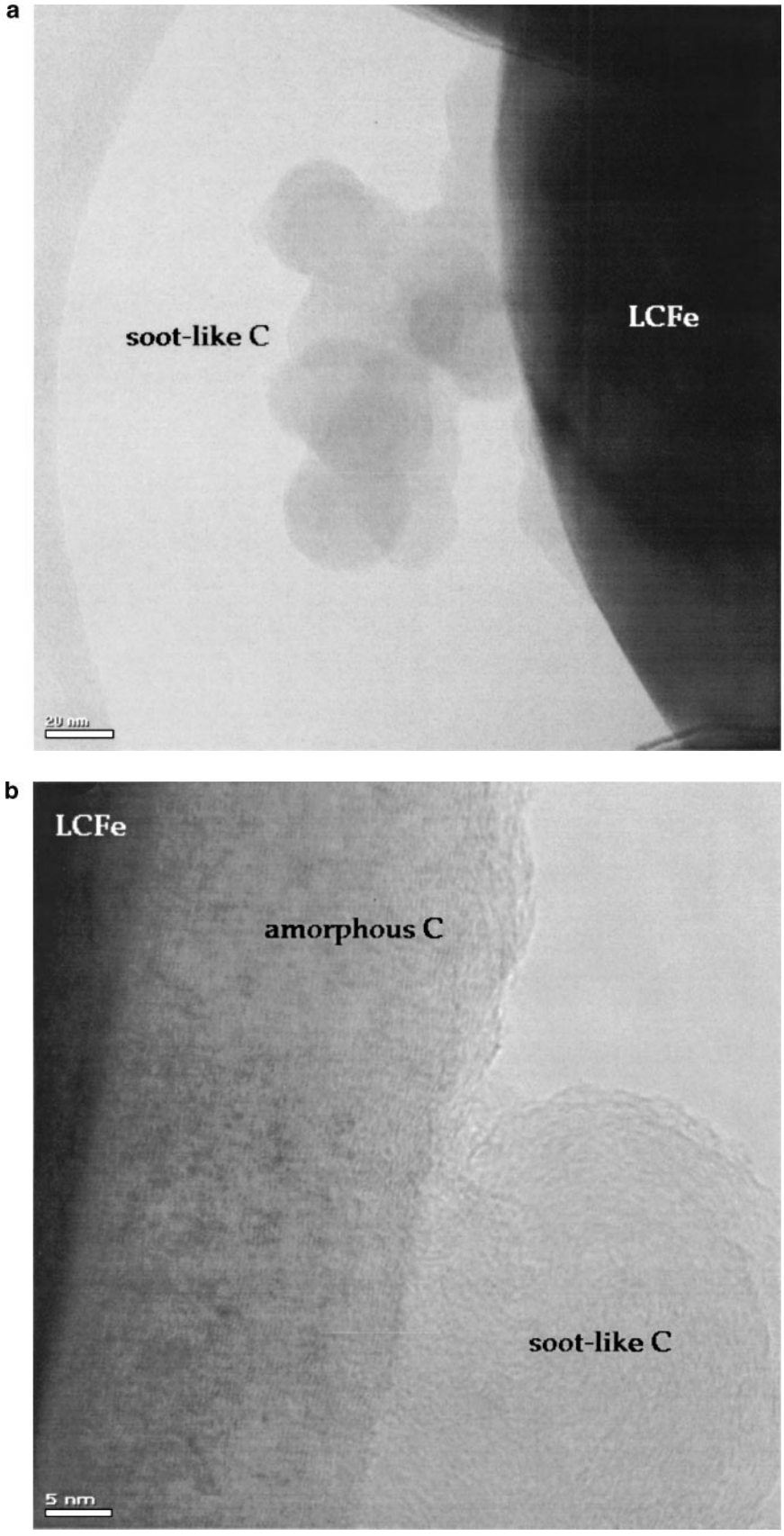

FIG. 8. TEM micrographs of different types of carbon over LCFe powders after catalytic runs in 56 : 41 : 3 CH_4 : Ar : H_2O; (a) soot-like carbon and (b) amorphous carbon films of ≈20 nm thick at 850°C; (c) graphitic carbon and (d) filaments at 900°C.

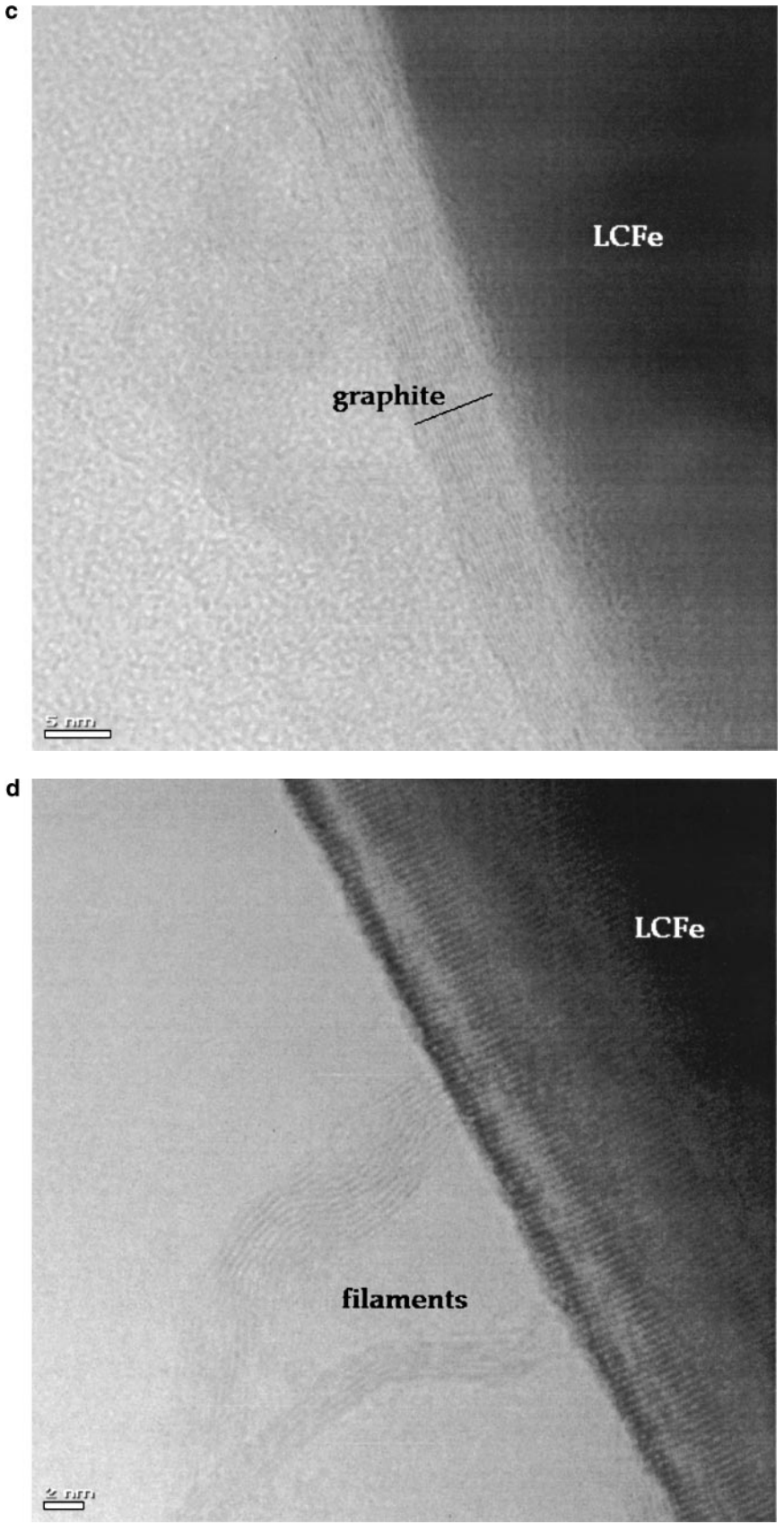

FIG. 8—*Continued*

and $CaCr_2O_4$, were indeed observed on the LCaCNi powder and, in some cases, they were attached to Ni islets (see Fig. 6). The XPS results indicate no surface segregation for Ni. This clearly indicates that the catalytic activity of the LCaCNi is not directly related to the Ni islets as the LCNi has a similar catalytic behavior.

XRD, XPS, and TEM measurements conducted on freshly prepared as well as on tested LCNi and LCaCNi powders, showed no change in the composition due to catalysis. This is also true for the iron-substituted catalyst based on XPS and TEM data and for the other transition-metal-substituted catalysts based on XRD and XPS measurements. On the other hand, Ca and Sr segregation measured by XPS was significant, as observed in the past (17, 18). XPS analysis on LCaCNi powders, exposed to different atmospheres (wet H_2, CO_2, and air), show clearly the effect of wet hydrogen on Ca segregation (see Table 4). Interestingly, Ni did not segregate during these tests. Preliminary thermodynamic calculations show that H_2 and H_2O lead to a higher loss of Sr and Ca due to the formation of volatile hydroxyl species, whereas CO, CO_2 and O_2 have almost no effect. Our results may indicate that the Ca and Sr solubilities are below 15% of the La site. Sfeir *et al.* (18) and Peck *et al.* (27) have reported a value for Sr in LC of 15% at 850°C and of 10% at 950°C, respectively, whereas Carter *et al.* (30) and Sfeir *et al.* (18) indicate a solubility limit for Ca in LC of 20% at 900°C and 15% at 800°C, respectively. Moreover, Mg, Mn, Fe, Co, and Ni do not segregate further after the catalytic runs, indicating that they may not destabilize the perovskite structure. This is in accordance with TPR results, which shows clearly that all of the LC catalysts did not undergo total reduction of the *B* site substitutent. Our thermodynamic calculations based on the ideal solid solution model used by Yokokawa *et al.* (31) indicate further that the Fe- and Ni-substituted LCs would decompose at a pO_2 of 1.26×10^{-23} and 3.16×10^{-16}, respectively, to yield the metal and the $LaCrO_3$ phase, while Mg, Ca, Sr, Mn, and Co would decompose to the metal oxide and $LaCrO_3$ phases at a pO_2 of 1.6×10^{-14}, 1.0×10^{-19}, 1.6×10^{-26}, 6.3×10^{-24}, and 1.9×10^{-14}, respectively (29). Our present experimental results suggest that the decomposition of LCs is hindered kinetically.

If we try to correlate the XPS observations with the apparent activities of the different LCs, we observe that in the 5 : 1 $CH_4 : O_2$ gas mixture, the activity follows the trend of the O_{II} and O_I BE, i.e., the activity increases with the strength of the oxygen adsorption, and the easiness of reduction of the lattice. Overall, the change in activity with the substitution, if expressed as TOF, is observed to be very marginal in the case of Mg, Ca, Sr, and Mn. For Fe, Co, and Ni, the substitution induces a higher activity when compared to the LC base material. For the Mn and Co substitution the activity is lower than in the base materials, $LaMnO_3$ and $LaCoO_3$, where higher valencies, Mn^{IV} and Co^{IV}, are formed upon substitution with Sr or Ca (e.g., at 850°C, TOF $\approx 2 \times 10^{-6}$ and 8×10^{-9} moles of CH_4/m^2 s for methane oxidation on $La_{0.8}Sr_{0.2}CoO_3$ and $LaCr_{0.9}Co_{0.1}O_3$, respectively (6)). This could be due to the low valencies of Mn and Co in LC (Mn^{III} and $Co^{III,II}$). Also, a double substitution with Ca or Sr and a *B* site substitutent has an effect on the activity. The TOF increases from 5.1×10^{-9} for LCMg to 9.8×10^{-9} for LCaCMg, but stays constant for Ni-substituted LC, being of 1.9×10^{-8} for LCNi and 2.1×10^{-8} for LCaCNi at 850°C, in 5 : 1 $CH_4 : O_2$. This could also be correlated with the conductivities of the catalysts (1 to 1.27 S/cm for LCaCMg and LSrCMg versus 0.16 S/cm for LCMg, and 1.91 S/cm for LCaCNi versus 0.39 S/cm for LCNi, in wet hydrogen), related to higher hole and oxygen vacancies conductivities.

A thorough analysis of the product distribution in the case of the methane-steam reaction indicates that the main reaction is steam reforming leading to CO and H_2. When going from 3 to 23% water, the CO selectivity was reduced (see Table 3). In most cases water has no influence on the CH_4 conversion, so that this change in selectivity is related to a fast reverse water–gas shift reaction (reaction [3]). The order of the reaction for water is near zero and it changes from negative to positive values with temperature. The activation energy of the reaction also increases with the steam content. This could be related to the competitive coverage of adsorbed species on multiple sites (32). Only the Ni and Sr substitutions seem to increase CH_4 conversion, indicating that these substituents do promote CH_4 dissociation. The low conversion of methane in the other substitutions is thought to be responsible for the low OCVs (open circuit voltages) measured with these anodes in SOFC tests. The situation seems to be similar to gold anodes (OCV $\approx$ 700 mV). Theoretical OCVs for cells using air at the cathode and a 56 : 41 : 3 $CH_4 : Ar : H_2O$ gas mixture at different anodes, were calculated (see Table 5)

TABLE 5

Estimated OCVs, in 56 : 41 : 3 $CH_4 : Ar : H_2O$, at 800°C, Were Calculated from the Exhaust Gas Composition by Considering the Unreacted CH_4 to be Equivalent to Ar

Catalyst composition	pO_2 [atm]	OCV [mV]
Theoretical	$4.80E^{-24}$	1205
$La_{0.85}Ca_{0.15}CrO_3$	$3.76E^{-19}$	944
$La_{0.85}Ca_{0.15}Cr_{0.9}Mg_{0.1}O_3$	$3.68E^{-18}$	892
$La_{0.85}Ca_{0.15}Cr_{0.9}Ni_{0.1}O_3$	$1.81E^{-23}$	1174
$La_{0.85}Sr_{0.15}CrO_3$	$7.11E^{-21}$	1036
$La_{0.85}Sr_{0.15}Cr_{0.9}Mg_{0.1}O_3$	$5.96E^{-18}$	881
$LaCrO_3$	$1.32E^{-18}$	915
$LaCr_{0.9}Mg_{0.1}O_3$	$1.17E^{-16}$	812
$LaCr_{0.9}Mn_{0.1}O_3$	$3.92E^{-19}$	943
$LaCr_{0.9}Fe_{0.1}O_3$	$7.80E^{-19}$	928
$LaCr_{0.9}Co_{0.1}O_3$	$1.19E^{-17}$	865
$LaCr_{0.9}Ni_{0.1}O_3$	$7.29E^{-22}$	1089

based on the actual exhaust gas composition, using HSC thermodynamic equilibria calculation software (Outokumpu Research Oy, Finland). For the calculation, the unreacted CH_4 was considered to be inert and equivalent to Ar. The calculated OCV of 880 and 914 mV at 800°C for LSrCMg and LCaCMg is close to the measured values of 862 and 892 mV, respectively. These OCVs agree well when considering the oxygen partial pressure determined by the P_{H_2O}/P_{H_2} and P_{CO_2}/P_{CO} equilibria from the $H_2 + \frac{1}{2}O_2 = H_2O$ and $CO + \frac{1}{2}O_2 = CO_2$ reactions. The theoretical OCV for the CH_4 reaction is 1205 mV at 800°C. Impedance spectroscopy measurements done during electrochemical tests at OCV show that the reaction sequences had the same order of reaction for H_2 and CH_4, whereas the activation energies were different. This indicates that the reactions are governed by CH_4 activation followed by the removal of the carbonaceous species on the catalyst surface to form syngas.

A simplified reaction sequence could be proposed (33) as

$$H_2O(g) + V_o^{\bullet\bullet} + O_o^x = 2(OH)_o^{\bullet} \quad [6]$$

$$2(OH)_o^{\bullet} = H_2 + 2h^{\bullet} + 2O_o^x \quad [7]$$

$$O_o^x + h^{\bullet} = O_o^{\bullet} \quad [8]$$

$$CH_4 + O_o^{\bullet} \rightarrow {}^{\bullet}CH_3 + (OH)_o^{\bullet} \quad [9]$$

$$CH_4 + (OH)_o^{\bullet} + h^{\cdot} \rightarrow {}^{\bullet}CH_3 + (H_2O)_o^{\bullet\bullet} \quad [10]$$

$$(H_2O)_o^{\bullet\bullet} \rightarrow H_2O(g) + V_o^{\bullet\bullet} \quad [11]$$

$$CH_{x(ads)} + H_2O = CO + [1 + x_{/2}]H_2 \quad [12]$$

$$CO + H_2O = CO_2 + H_2 \quad [3]$$

with reactions [6], [8], and [9] in competition with each other, $V_o^{\bullet\bullet}$, O_o^x, $O_o^{\bullet}$, $(OH)_o^{\bullet}$, $(H_2O)_o^{\bullet\bullet}$, $h^{\bullet}$, ${}^{\bullet}CH_3$ representing the doubly charged oxygen ion vacancy, the oxygen O^{--} and O^- on the normal lattice position, a positive hydroxyl-group on regular oxygen position, a doubly charged adsorbed water molecule, the electron hole in valence band, and a methyl radical, respectively. Part of this sequence could also explain the oxidative coupling of CH_4 related to the Mg-based catalysts. Mg enhances the coupling reaction of LC, probably by radical formation. MgO is known as a good coupling catalyst (34). The coupling activity is further enhanced in LC when a double substitution with Mg and Ca or Sr is considered. This is related to the increase in the hole conductivity and in the vacancy concentration, increasing thus the possibility to form $O_o^{\bullet}$ active sites. The increase of the steam content blocks these active sites. On the other hand, Ni substitution promotes the dissociation of methane and its subsequent reaction with water to syngas.

Finally, the TPO results show the very low carbon coverage on lanthanum chromites, except for the LCFe powder. This indicates that these materials withstand coking and do not seem to promote it. Even in the case of the most active catalyst in our study (LCaCNi), carbon did not build up with time, and most of it is related to the presence of the free Ni-islets. The activity is moreover sustained for more than 360 h, indicating that carbon formation does not seem to poison the catalytic sites of the LCaCNi powder. Also, comparing the TPO results with TEM analysis shows that a pronounced TPO peak at 829°C observed for the LCFe powder could be related to graphitic carbon, whereas on Ni-substituted LCs we observe some amorphous carbon (580–600°C) and thin film graphite (620–790°C). The low temperature peaks could be related to low coverage adsorbed carbon species like methane or related radicals. Another observation is that the type of carbon does not seem to vary a lot with the gas mixture used.

Fuel cell measurements using anodes of $La_{0.85}Sr_{0.15}Cr_{0.9}Ni_{0.1}O_3$ and $La_{0.85}Sr_{0.15}CrO_3$ on YSZ electrolyte, showed interesting results with both hydrogen and methane fuels. A power density of 140 mW/cm^2 was achieved with both fuels at 900°C in the case of LSrCNi. LSrC showed a similar power output in hydrogen but gave only half of that value in methane. Studies are in progress to improve the electrode–electrolyte interface to attain higher power densities. This initial result indeed proves that similar power output could be achieved by using either H_2 or CH_4. The electrochemical data further indicates that by suitably substituting a stable material like $LaCrO_3$, it is possible to improve not only their catalytic activity but also their electrochemical behavior.

CONCLUSIONS

By substituting the inactive $LaCrO_3$ catalyst with alkaline earth and first series transition metal elements, a noticeable improvement in activity toward methane conversion is achieved. For the $LaCrO_3$ compounds, three different behavioral patterns were observed depending on the catalyst composition. It was observed that among the alkaline earth elements, Mg had an inhibiting effect, whereas Ca and Sr substitution improved the catalytic activity for CH_4 oxidation, and CO_2 and H_2O reforming reactions. Transition metal substitution experiments on the *B* site indicate that Co has an inhibiting effect, whereas Mn and Fe showed an enhancement in activity when compared to the activity of the base material, $LaCrO_3$. The $LaCrO_3$ activity is however not modified drastically. On the other hand, Ni substitution causes a considerable change in the turn over frequency (fourfold when compared to $LaCrO_3$). Among the transition-metal substituents, Co and Mn showed the lowest cracking activity, whereas Fe deposited high amounts of C. Thus by suitable substitution of the stable but inactive $LaCrO_3$ catalyst with Ni, we have been able to produce an improved catalyst for CH_4 oxidation with low coking activity for their use as a SOFC anode material. Also, all these

experiments were done in methane-rich atmospheres, simulating real SOFC conditions.

ACKNOWLEDGMENTS

We are grateful for the financial support of the European Brite/Euram project BRPR-CT97-0413 and the Japanese NEDO 98-EF2 project. One of the authors (R.V.) has been partially supported by the Swiss Federal Energy Office (OFEN/BfE–Project EMPA Thun). Many thanks are also due to Hugh Middleton for his fruitful discussions and Augustin J. McEvoy for providing laboratory facilities.

REFERENCES

1. Ledjeff, K., Rohrbach, T., and Schaumberg, G., *in* "Second International Symposium on Solid Oxide Fuel Cells," p. 323. Athens, Greece, 1991.
2. Marti, P. E., Ph.D. thesis, p. 135, Swiss Federal Institute of Technology Zürich, Zürich, 1994.
3. Tejuca, L. G., Fierro, J. L. G., and Tascon, J. M. D., *Adv. Catal.* **36**, 237 (1989).
4. Chan, K. S., Ma, J., Jaenicke, S., and Chuah, G. K., *Appl. Catal. A: General* **107**, 201 (1994).
5. Doshi, R., Alcock, C. B., Gunasekaran, N., and Carberry, J. J., *J. Catal.* **140**, 557 (1993).
6. Seiyama, T., *Catal. Rev.-Sci. Eng.* **34**, 281 (1992).
7. Nakamura, T., Petzow, G., and Gauckler, L. J., *Mat. Res. Bull.* **14**, 649 (1979).
8. Arai, H., Yamada, T., Eguchi, K., and Seiyama, T., *Appl. Catal.* **26**, 265 (1986).
9. Gunasekaran, N., Bakshi, N., Alcock, C. B., and Carberry, J. J., *Solid State Ionics* **83**, 145 (1996).
10. McCarty, J. G., and Wise, H., *Catal. Today* **8**, 231 (1990).
11. Fierro, J. L. G., Tascon, J. M. D., and Tejuca, L. G., *J. Catal.* **93**, 83 (1985).
12. Collongue, B. d., Garbowski, E., and Primet, M., *J. Chem. Soc. Faraday Trans.* **87**, 2493 (1991).
13. Saracco, G., Scibilia, G., A. I., and Baldi, G., *Appl. Catal. B: Environmental.* **8**, 229 (1996).
14. Stojanovic, M., Mims, C. A., Moudallal, H., Yang, Y. L., and Jacobson, A. J., *J. Catal.* **166**, 324 (1997).
15. Baker, R. T., and Metcalfe, I. S., *Appl. Catal. A: General.* **126**, 297 (1995).
16. Baker, R. T., and Metcalfe, I. S., *Appl. Catal. A: General.* **126**, 319 (1995).
17. Sfeir, J., Van herle, J., and McEvoy, A. J., *in* "Third European Solid Oxide Fuel Cell Forum," p. 267. Nantes-France, 1998.
18. Sfeir, J., Van herle, J., and McEvoy, A. J., *J. Eur. Ceram. Soc.* **19**, 897 (1999).
19. Levenspiel, O., "Chemical Reaction Engineering." Wiley, New York, 1999.
20. Armstrong, T. R., Stevenson, J. W., Pederson, L. R., and Raney, P. E., *J. Electrochem. Soc.* **143**, 2919 (1996).
21. Rostrup-Nielsen, J. R., *in* "Catalysis, Science and Technology" (J. R. Anderson, and M. Boudart, Eds.) Springer-Verlag, Berlin/New York, 1984.
22. Twigg, M. V., "Catalyst Handbook." Wolfe, New York, 1989.
23. Bartholomew, C. H., *Catal. Rev.-Sci. Eng.* **24**, 67 (1982).
24. Strohmeier, B. R., and Hercules, D. M., *J. Phys. Chem.* 4922 (1984).
25. Sugimoto, K., Seto, M., Tanaka, S., and Hara, N., *J. Electrochem. Soc.* **140**, 1586 (1993).
26. Helfland, M. A., Clayton, C. R., Diegle, R. B., and Sorenson, N. R., *J. Electrochem. Soc.* **139**, 2121 (1992).
27. Peck, D. H., Hilpert, K., Miller, M., Korbertz, D., and Nickel, H., "Untersuchungen zur Verdampfung und Thermodynamik von Perowskiten auf der Basis von $LaCrO_3$ für Hochtemperatur-Brennstoffzellen mot Festelektrolyt (SOFC)," Forschungszentrum Jülich GmbH, Institut für Werkstoffe der Energietechnik, (1996).
28. Yasuda, I., and Hishinuma, M., *J. Electrochem. Soc.* **143**, 1583 (1996).
29. Sfeir, J., Proceedings of "Solid Oxide Fuel Cell Materials and Mechanisms," IEA-ESF Joint topical meeting, Les Diablerets, Switzerland, Swiss Federal Office of Energy, Bern, 2001.
30. Carter, J. D., Sprenkle, V., Nasrallah, M. M., and Anderson, H. U., *in* "Third International Symposium on Solid Oxide Fuel Cells," p. 344. Honolulu, Hawaii, 1993.
31. Yokokawa, H., Sakai, N., Kawada, T., and Dokiya, M., *Solid State Ionics.* **52**, 43 (1992).
32. Frennet, A., Liénard, G., Crucq, A., and Degols, L., *J. Catal.* **53**, 150 (1978).
33. Gellings, P. J., and Bouwmeester, H. J. M., *Catal. Today.* **58**, 1 (2000).
34. Dubois, J. L., and Cameron, C. J., *Appl. Catal.* **67**, 49 (1990).